Journal of Magnetism and Magnetic Materials 349 (2014) 201–207

Contents lists available at ScienceDirect

Journal of Magnetism and Magnetic Materials

journal homepage: www.elsevier.com/locate/jmmm

Magnetic order of the La_3NiGe_2-type Tb_3NiSi_2

A.V. Morozkin [a,*], V. Svitlyk [b], Y. Mozharivskyj [b], O. Isnard [c]

[a] Department of Chemistry, Moscow State University, Leninskie Gory, House 1, Building 3, Moscow GSP-2 119992, Russia
[b] Department of Chemistry and Chemical Biology, McMaster University, 1280 Main Street West, Hamilton, Ontario, Canada L8S 4M1
[c] Institut Néel, CNRS – Université Joseph Fourier, Departement MCMF, 25 rue des Martyrs BP166x, 38042 Grenoble cedex 9, France

ARTICLE INFO

Article history:
Received 17 December 2012
Received in revised form
1 May 2013
Available online 5 September 2013

Keywords:
Rare earth intermetallic
Magnetic property
Neutron diffraction
Magnetic structure

ABSTRACT

The novel Tb_3NiSi_2 phase adopts the La_3NiGe_2-type structure (*Pnma*, *N 62*, *oP24*). According to the thermal dependence of the magnetization measurements in 100 Oe applied field, Tb_3NiSi_2 undergoes a ferromagnetic-like transition at 135 K and a spin-orientation transition at 53 K. Based on the neutron diffraction studies in a zero applied field, Tb_3NiSi_2 shows four types of mixed ferromagnetic–antiferromagnetic ordering below ~130 K, 82 K, 66 K and 53 K. The unit cell of Tb_3NiSi_2 undergoes an isotropic compression down to 143 K and an anisotropic one below the temperature of the ferromagnetic transition at ~130 K: the *a* cell parameter increases, whereas the *b* and *c* cell parameters and unit cell volume decrease with the decreasing temperature. At 1.5 K the terbium magnetic moment reaches the value 9.1(1) μ_B.

1. Introduction

The novel Tb_3NiSi_2 compound crystallizes with the La_3NiGe_2-type structure (space group *Pnma*, *N 62*, *oP24*). The La_3NiGe_2 structure is a member of the family of the two-layer orthorhombic structures with the *Pnma* symmetry and a set of special 4*c* sites (*x*, 1/4, *z*) derived from the hexagonal Mg structure [1]. The known La_3NiGe_2-type Pr_3CoGe_2 and Nd_3CoGe_2 phases undergo a mixed antiferro–ferromagnetic *ac*-plane ordering with the **Pn′ma** magnetic space group below 28 K and 35.5 K, respectively [2], whereas below 135 K Tb_3NiGe_2 demonstrates a *b*-axis ferrimagnetic ordering with the **Pnm′a** magnetic space group [3]. This work aims to understand the nature of the magnetic ordering in Tb_3NiSi_2 on the basis of both magnetic and neutron diffraction studies.

2. Experimental details

The Tb_3NiSi_2 sample was prepared by arc-melting the weighed amounts of terbium (99.9 wt%), nickel (99.95 wt%) and silicon (99.99 wt%). The sample was annealed at 1070 K for 175 h in an argon atmosphere and quenched in ice-cold water.

The quality of the samples was evaluated using powder X-ray diffraction (XRD) and X-ray spectral microprobe analysis. The XRD data were obtained on a DRON-3.0 diffractometer (CuK_α radiation, $2\Theta = 10–80^\circ$, step 0.05°, 4 s per step) at room temperature. The unit cell data were derived using the Rietan-program [4] in the isotropic approximation. A Camebax microanalyser was employed to perform microprobe X-ray spectral analysis of the sample (15 kV, 3×10^{-8} A, *K*-, *L*- and *M*-lines, 2×2 μm^2).

The temperature-dependant dc magnetization and saturation magnetization were measured on a commercial SQUID magnetometer (Quantum Design) in the 5–300 K range and in an applied field of up to 50 kOe.

The neutron diffraction experiments were carried out on the D1B powder diffractometer [5] ($\lambda = 0.252$ nm at the Institute Laue-Langevin, Grenoble, France). The neutron diffraction patterns were identified and calculated using the FULLPROF program and traditional crystallographic approach [6].

3. Results and discussion

3.1. Crystal structure

The quantitative microprobe X-ray analysis of the Tb_3NiSi_2 sample yielded the $Tb_{50(1)}Ni_{16(1)}Si_{34(2)}$ composition which is identical to the expected one. The crystallographic and atomic parameters of La_3NiGe_2-type Tb_3NiSi_2 are given in Table 1. Rietveld analysis of powder X-ray pattern indicates the mixed **T1** = $Ni_{0.9}Si_{0.1}$ and **T2** = $Ni_{0.1}Si_{0.9}$ atomic sites. The interatomic distances of Tb_3NiSi_2 are close to the sum of atomic (metallic) radius [7] and, thus, are indicative of the metallic type bonding in the structure (Table 2).

The plots for the **dc magnetization** and **inverse susceptibility** of the polycrystalline Tb_3NiSi_2 sample are given in Fig. 1. According

* Corresponding author. Tel.: +7 849 593 93472.
E-mail address: morozkin@general.chem.msu.ru (A.V. Morozkin).

0304-8853/$ - see front matter © 2013 Elsevier B.V. All rights reserved.
http://dx.doi.org/10.1016/j.jmmm.2013.08.052

to the magnetization data, Tb_3NiSi_2 undergoes a ferromagnetic-type transition at 135 K and spin orientation at ~52 K. The paramagnetic susceptibility follows the Curie–Weiss law in the temperature range from 150 to 350 K. The fit to the Curie–Weiss law in this region gives a positive Weiss temperature $\Theta_p = 127$ K suggesting **dominant ferromagnetic interactions**. The effective magnetic moment per formula unit M_{eff}/f.u. of 16.3 μ_B yields an effective magnetic moment of 9.41 μ_B per Tb atom which is in good agreement with the theoretical value of 9.72 μ_B for Tb^{3+} [8]. These data also suggest that Ni atoms carry no magnetic moment.

3.1.1. *Neutron diffraction study of La_3NiGe_2-type Tb_3NiSi_2 crystal structure*

The La_3NiGe_2-type Tb_3NiSi_2 structure (space group *Pnma*, point group $\mathbf{D}_{2h}$) consists of the 4c sites for the terbium, nickel and silicon atoms (Table 1). Such a two-layer structure with the *Pnma* space group may be given in terms of the orthorhombic $Pna2_1$ (point group $\mathbf{C}_{2v}$), $P2_12_12_1$ (point group $\mathbf{D}_2$) or monoclinic $P2_1/n$ (point group $\mathbf{C}^x_{2h}$) and $P2_1/a$ (point group $\mathbf{C}^z_{2h}$) space groups in case of the orthorhombic ($y/b = 1/4 \rightarrow y/b \neq 1/4$) or monoclinic distortion of the unit cell. The symmetry operators for the corresponding point and space groups and *4c* atomic positions of the terbium sublattice are given in Table 3. These "colorless" $\mathbf{D}_2$, $\mathbf{C}_{2h}$ and $\mathbf{C}_{2v}$ point groups and "black–white" $\mathbf{D}'_2$, $\mathbf{C}'_{2h}$ and $\mathbf{C}'_{2v}$ magnetic point groups [9–11] were used for the analysis of neutron diffraction data.

Table 1
Atomic positions in the La_3NiGe_2-type Tb_3NiSi_2 phase ($a = 1.1308(1)$ nm, $b = 0.41314(3)$ nm, $c = 1.1225(1)$ nm, space group *Pnma, No. 62, Z*=4, atomic displacement parameters for all atoms $\beta_{11} = 0.001955$, $\beta_{22} = 0.014647$ and $\beta_{33} = 0.001984$ at 298 K, $R_F = 3.1\%$).

Atom	Site	*x/a*	*y/b*	*z/c*	Occupancy
Tb1	*4c*	0.3781(5)	1/4	0.4350(5)	1.00
Tb2	*4c*	0.0564(5)	1/4	0.3782(5)	1.00
Tb3	*4c*	0.2104(5)	1/4	0.7023(6)	1.00
T1[a]	*4c*	0.1338(7)	1/4	0.1294(7)	1.00
Si1	*4c*	0.4905(9)	1/4	0.6748(9)	1.00
T2[a]	*4c*	0.3051(9)	1/4	0.0057(9)	1.00

[a] **T1** = $Ni_{0.9}Si_{0.1}$; **T2** = $Ni_{0.1}Si_{0.9}$.

The unit cell of Tb_3NiSi_2 undergoes isotropic compression down to 143 K and anisotropic one below the temperature of ferromagnetic transition: $\Delta a/a_{174\ K} > \Delta b/b_{174\ K} \approx \Delta c/c_{174\ K}$ and as well as below 117 K: $\Delta a/a_{174\ K} > \Delta b/b_{174\ K} > \Delta c/c_{174\ K}$. Contrary to the *b* and *c* cell parameters, the *a* cell parameter increases with decreasing temperature (Fig. 2a). At 1.5 K the $\Delta a/a_{174\ K}$, $\Delta b/b_{174\ K}$ and $\Delta c/c_{174\ K}$ ratios reach the values of 0.00231, −0.00206 and −0.00339, respectively; whereas $\Delta V/V_{174} = -0.00316$. The temperatures of the local maxima in the *V–T* plot coincide with the transformation temperatures of the Tb_3NiSi_2 magnetic structure (Fig. 2b). Such behavior in the lattice parameters must result from the magnetic ordering.

Based on the present powder neutron diffraction study, there are no obvious reasons to reduce the *Pnma* symmetry of the Tb_3NiSi_2 lattice to the $Pna2_1$, $P2_12_12_1$, $P2_1/n$ or $P2_1/a$ ones as the temperature decreases from 174 K down to 1.5 K.

3.1.2. *Magnetic structure*

The set of commensurate and incommensurate magnetic reflections was used to derive the magnetic ordering of Tb_3NiSi_2 (Fig. 3). The thermal variation of the strongest (1/2 0 0), (1/4 0 3/4), (100)

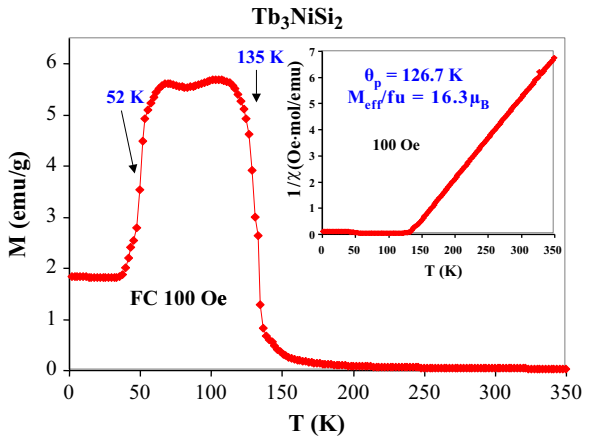

Fig. 1. Magnetization (FC) and inverse magnetic susceptibility as a function of temperature in the 100 Oe field.

Table 2
Interatomic distances for Tb_3NiSi_2. Their ratio to the sum of the atomic radii of the corresponding atoms ($R_{Tb} = 0.17788$ nm, $R_{Ni} = 0.12459$ nm, $R_{Si} = 0.1176$ nm, $R_{T1} = 0.9 \cdot R_{Ni} + 0.1 \cdot R_{Si} = 0.12389$ nm, $R_{T2} = 0.1 \cdot R_{Ni} + 0.9 \cdot R_{Si} = 0.11830$ nm) [7] is given as $\Delta = D/(R_{atom1} + R_{atom2})$. δ is a coordination number. The shortest Tb–Tb distances are shown in bold. T1 = $Ni_{0.9}Si_{0.1}$, T2 = $Ni_{0.1}Si_{0.9}$.

Atom-	Atom	*D*, nm	Δ	Atom-	Atom	*D*, nm	Δ	Atom-	Atom	D, nm	Δ
Tb1-	1Si1	0.28274	0.96	Tb2-	1T1	0.29267	0.97	Tb3-	2T1	0.28356	0.94
	1Si1	0.29767	1.01		2T2	0.29611	1.00		1Si1	0.28437	0.96
	1T1	0.29805	0.99		2Si1	0.31243	1.06		2T2	0.30279	1.02
	2T1	0.30078	1.00		1T2	0.31263	1.06		1Si1	0.31824	1.08
	2T2	0.30313	1.02		2Tb2[a]	**0.36567**	1.03		2Tb1[a]	**0.34773**	0.98
	2Tb3[a]	**0.34773**	0.98		1Tb1[a]	0.36932	1.04		1Tb1[a]	0.35495	1.00
	1Tb3[a]	0.35495	1.00		2Tb3	0.37664	1.06		1T2	0.35701	1.21
	1Tb2[a]	0.36932	1.04		2Tb3	0.38884	1.09		2Tb2	0.37664	1.06
	2Tb1	0.37413	1.05		1Tb3[a]	0.40333	1.13		2Tb2	0.38884	1.09
	1Tb2	0.40528	1.14		1Tb1	0.40528	1.14		1Tb2[a]	0.40333	1.13
	2Tb1	0.41314	1.16		2Tb2	0.41314	1.16		2Tb3	0.41314	1.16
		δ = 17				**δ = 17**				**δ = 17**	
T1-	1T2	0.23833	0.98	Si1−-	2T1	0.25500	1.03	T2-	1T1	0.23833	0.98
	2Si1	0.25500	1.03		2Tb1	0.28274	0.96		2Tb2	0.29611	1.00
	2Tb3	0.28356	0.94		1Tb3	0.28437	0.96		2Tb3	0.30279	1.02
	1Tb2	0.29267	0.97		1Tb1	0.29767	1.01		2Tb1	0.30313	1.02
	1Tb1	0.29805	0.99		2Tb2	0.31243	1.06		1Tb2	0.31263	1.06
	2Tb1	0.30078	1.00		1Tb3	0.31824	1.08		1Tb3	0.35701	1.21
		δ = 9				**δ = 9**				**δ = 9**	

[a] The bond is shown in Fig. 5c and h.

Table 3
Atomic positions for the *4c* sites of the *Pnma*[a] space group (retained by Tb_3NiSi_2) with the corresponding symmetry operators and subgroups.

No.	Atom	*y*/*b*	*x*/*a*	*z*/*c*	Symmetry operator	Point subgroup of *4c* site			
						D_2[b]	C_{2v}[c]	C_{2h}[d]	C_{2h}[e]
1	$Tb1^1$, $Tb2^1$, $Tb3^1$	1/4	*x*	*z*	{**1**, $\mathbf{m}_y$/[0 1/2 0]}	**1**	**1**	1	**1**
2	$Tb1^2$, $Tb2^2$, $Tb3^2$	3/4	1/2−*x*	1/2+*z*	{$\mathbf{2}_z$/[1/2 0 1/2], $\mathbf{m}_x$/[1/2 1/2 1/2]}	$\mathbf{2}_z$	$\mathbf{m}_x$	$\mathbf{m}_x$	$\mathbf{2}_z$
3	$Tb1^3$, $Tb2^3$, $Tb3^3$	1/4	1/2+*x*	1/2−*z*	{$\mathbf{m}_z$/[1/2 0 1/2], $\mathbf{2}_x$/[1/2 1/2 1/2]}	$\mathbf{2}_x$	$\mathbf{m}_z$	$\mathbf{2}_x$	$\mathbf{m}_z$
4	$Tb1^4$, $Tb2^4$, $Tb3^4$	3/4	−*x*	−*z*	{$\bar{\mathbf{1}}$, $\mathbf{2}_y$/[0 1/2 0]}	$\mathbf{2}_y$	$\mathbf{2}_y$	$\bar{\mathbf{1}}$	$\bar{\mathbf{1}}$

[a] For two-layer structures: *Pnma*(*x*, *y*, *z*)={**1**, $\mathbf{m}_y$/[0 1/2 0]} × {*Pna*2_1(*x*, *y*, *z*), *P*$2_12_12_1$(*x*, *y*, *z*), *P*2_1/*n*(*x*, *y*, *z*), *P*2_1/*a*(*x*, *y*, *z*)};
[b] Space group *P*$2_12_12_1$={**1**, $\mathbf{2}_x$/[1/2 1/2 1/2], $\mathbf{2}_y$/[0 1/2 0], $\mathbf{2}_z$/[1/2 0 1/2]};
[c] Space group *Pna*2_1={**1**, $\mathbf{m}_x$/[1/2 1/2 1/2], $\mathbf{m}_z$/[1/2 0 1/2], $\mathbf{2}_y$/[0 1/2 0]};
[d] Space group *P*2_1/*n*={**1**, $\mathbf{m}_x$/[1/2 1/2 1/2], $\mathbf{2}_x$/[1/2 1/2 1/2], $\bar{\mathbf{1}}$};
[e] Space group *P*2_1/*a*={**1**, $\mathbf{m}_z$/[1/2 0 1/2], $\mathbf{2}_z$/[1/2 0 1/2], $\bar{\mathbf{1}}$}.

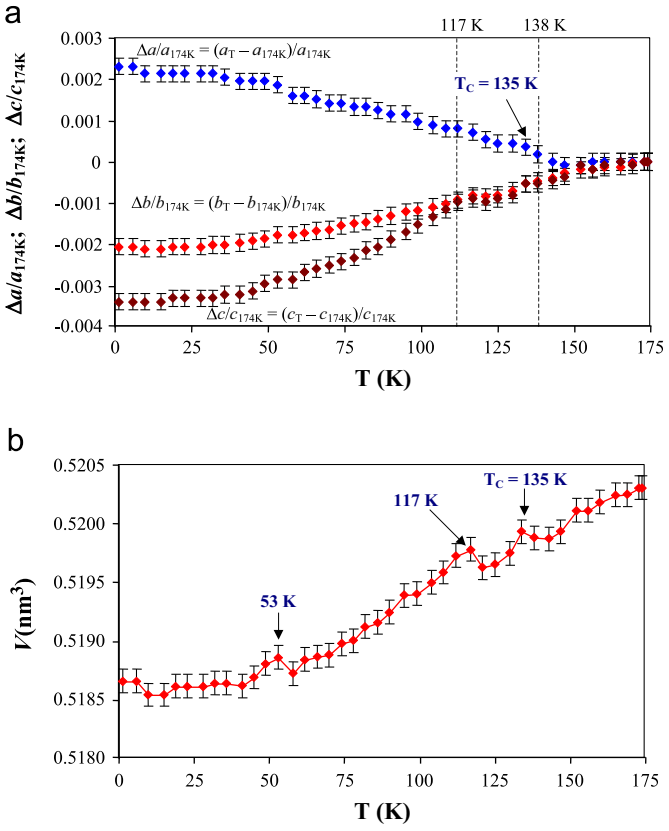

Fig. 2. (a) The relative cell parameters of Tb_3NiSi_2 vs. temperature and (b) unit cell volume of Tb_3NiSi_2 vs. temperature. Below 143 K and 117 K the anisotropic distortion of the unit cell is observed. The local maxima in the *V*–*T* plot coincide with the transformation temperatures of the Tb_3NiSi_2 magnetic structure.

and (302) magnetic reflection indicates transformation of the magnetic structure below ~130, 82, 66 and 53 K (Fig. 4). The ordering temperature of the ferromagnetic-type structure at ~130 K is close to that of 135 K obtained from the magnetization measurements (see above).

Between ~130 K and 82 K, the magnetic structure of Tb_3NiSi_2 is a sum of the $\mathbf{M}_{ac}^{K0}$ and M_b^{K0} magnetic components and the magnetic unit cell $a_{Tb3NiSi2} \times b_{Tb3NiSi2} \times c_{Tb3NiSi2}$ equals the crystal unit cell (wave vector $\mathbf{K}_0$=[0, 0, 0]). The *ac*-plane magnetic component $\mathbf{M}_{ac}^{K0}$ of the **Pn′ma**={**1**, 1′ × $\mathbf{m}_x$/[1/2 1/2 1/2]} × {**1**, $\mathbf{m}_y$/[0 1/2 0]} × {**1**, $\mathbf{m}_z$/[1/2 0 1/2]} magnetic space group and the *b*-axis magnetic component $\mathbf{M}_b^{K0}$ of the **Pnm′a**={**1**, $\mathbf{m}_x$/[1/2 1/2 1/2]} × {**1**, 1′ × $\mathbf{m}_y$/[0 1/2 0]} × {**1**, $\mathbf{m}_z$/[1/2 0 1/2]} one are given in Fig. 5a and c. The corresponding neutron diffraction pattern and image of the Tb_3NiSi_2 magnetic structure are given in Fig. 3b and Fig. 5d and e. The sum $\mathbf{M}_{ac}{}^{K0}$ (**Pn′ma**) and $\mathbf{M}_b^{K0}$(**Pnm′a**) magnetic components may be shown in term of the **P2′$_1$**/*a* magnetic space group: $\mathbf{M}_{ac}^{K0}$(**Pn′ma**)+$\mathbf{M}_b^{K0}$(**Pnm′a**)=($\mathbf{M}_{ac}^{K0}$+M_b^{K0})(**P2′$_1$**/*a*) and **P2′$_1$**/*a*={**1**, $\mathbf{m}_z$/[1/2 0 1/2], 1′ × $\mathbf{2}_z$/[1/2 0 1/2], 1′ × $\bar{\mathbf{1}}$}.

Below 82 K the $\mathbf{M}_b^{K0}$(**Pnm′a**) component vanishes and down to 66 K the magnetic structure of Tb_3NiSi_2 equals the $\mathbf{M}_{ac}^{K0}$(**Pn′ma**) magnetic component (magnetic unit cell $a_{Tb3NiSi2} \times b_{Tb3NiSi2} \times c_{Tb3NiSi2}$) (Figs. 3 and 5c). At 66 K the vague low-angle peak (perhaps the set of incommensurate peaks) converts to the clear (1/2, 0, 0) peak (see Fig. 3b, c and d) that indicates transformation of the magnetic structure and increase of the magnetic unit cell to $2a_{Tb3NiSi2} \times b_{Tb3NiSi2} \times c_{Tb3NiSi2}$ (Fig. 3d). Down to 53 K, the magnetic structure of Tb_3NiSi_2 is a sum of the $\mathbf{M}_{ac}^{K0}$(**Pn′ma**) and *b*-axis $\mathbf{M}_b^{K1}$ magnetic components with $\mathbf{K}_1$=[1/2, 0, 0] wave vector. The magnetic structure became a set of canted Tb magnetic moments with ferromagnetic ordering along the *a* axis and antiferromagnetic one in the *bc* plane (Fig. 5f and g).

The low angle [1/4, 0, 3/4] magnetic reflection below 53 K indicates an increase of the magnetic unit cell to $8a_{Tb3NiSi2} \times b_{Tb3NiSi2} \times 4c_{Tb3NiSi2}$ and appearance of a flat spiral $\mathbf{M}^{K2}$ magnetic component in the magnetic ordering of Tb_3NiSi_2 (Fig. 3e). The Tb_3NiSi_2 magnetic structure is now composed of canted ferromagnetic cones and is the sum of $\mathbf{M}_{ac}^{K0}$ (**Pn′ma**), $\mathbf{M}_b^{K1}$ and $\mathbf{M}^{K2}$ magnetic components ($\mathbf{K}_2$=[±1/4, 0, ±3/4] and the cone axis of the $\mathbf{M}^{K2}$ flat spiral component coincides with the ($\mathbf{M}_{ac}^{K0}$+$\mathbf{M}_b^{K0}$+$\mathbf{M}_b^{K1}$) vector of the corresponding Tb atom) (Fig. 5h).

The magnetic ordering of the Tbj^i atom (see Table 3) from ~130 to 1.5 K can be given as

$$\mathbf{M}_{Tbji} = \mathbf{i} \cdot \mathbf{M}_{ac}^{K0} \cdot \sin(\theta(\mathbf{M}_{ac}^{K0})) + \mathbf{j} \cdot [M_b^{K0} + M_b^{K1} \cdot \cos(\pi m)] + \mathbf{k} \cdot \mathbf{M}_{ac}^{K0} \cdot \cos(\theta(\mathbf{M}_{ac}^{K0})) + M^{K2} \cdot [\mathbf{i}' \cdot \cos(\pi m/2 + x_{Tbji}/4 + 3\pi n/2 + 3z_{Tbji}/4) + \mathbf{j} \cdot \sin(\pi m/2) + x_{Tbji}/4 + 3\pi n/2 + 3z_{Tbji}/4)],$$

here *m* and *n* are the number of the unit cells along the *a* and *c* axes, respectively (*m* and *n*=0…1, 2…); **i**, **j** and **k** are the orthonormal vectors (**i** coincides with the *a* axis, **j** with the *b* axis and **k** with the *c* axis). The cone axis of a flat spiral with the $\mathbf{K}_2$ wave vector coincides with the **k′** vector ($\mathbf{k}' = [\mathbf{i} \cdot \mathbf{M}_{ac}^{K0} \cdot \sin(\theta(\mathbf{M}_{ac}^{K0})) + \mathbf{j} \cdot [M_b^{K0} + M_b^{K1} \cdot \cos(\pi m)] + \mathbf{k} M_{ac}^{K0} \cdot \cos(\theta(\mathbf{M}_{ac}^{K0}))]/|\mathbf{i} \cdot \mathbf{M}_{ac}^{K0} \cdot \sin(\theta(\mathbf{M}_{ac}^{K0})) + \mathbf{j} \cdot [\mathbf{M}_b^{K0} + \mathbf{M}_b^{K0}\mathbf{M}_b^{K1} \cdot \cos(\pi m)] + \mathbf{k} \cdot \mathbf{M}_{ac}^{K0} \cdot \cos(\theta(\mathbf{M}_{ac}^{K0}))|$, **i′**, **j′** and **k′** are the orthonormal vectors. The magnetic components are listed in Table 4. Thermal evolution of the $\mathbf{M}_b^{K0}$, $\mathbf{M}_{ac}^{K0}$, $\mathbf{M}_b^{K1}$ and $\mathbf{M}^{K2}$ magnetic components of Tb_3NiSi_2 and the overal $|\mathbf{M}_{Tb}|$ terbium magnetic moment are given in Fig. 6. At 1.5 K, the terbium magnetic moments reach values of 9.1(1) μ_B, which agrees with the 9 μ_B value expected for the free Tb^{3+} ion [8] (Table 4).

In the zero applied field, Tb_3NiSi_2 demonstrates a complex mixed ferromagnetic–antiferromagnetic ordering. In summary, the sequence of magnetic ordering in Tb_3NiSi_2 is as follows: Paramagnet (symmetry $\mathbf{D}_{2h}$, *Pnma*, size of the unit cell is $a_{Tb3NiSi2} \times b_{Tb3NiSi2} \times c_{Tb3NiSi2}$)→mixed

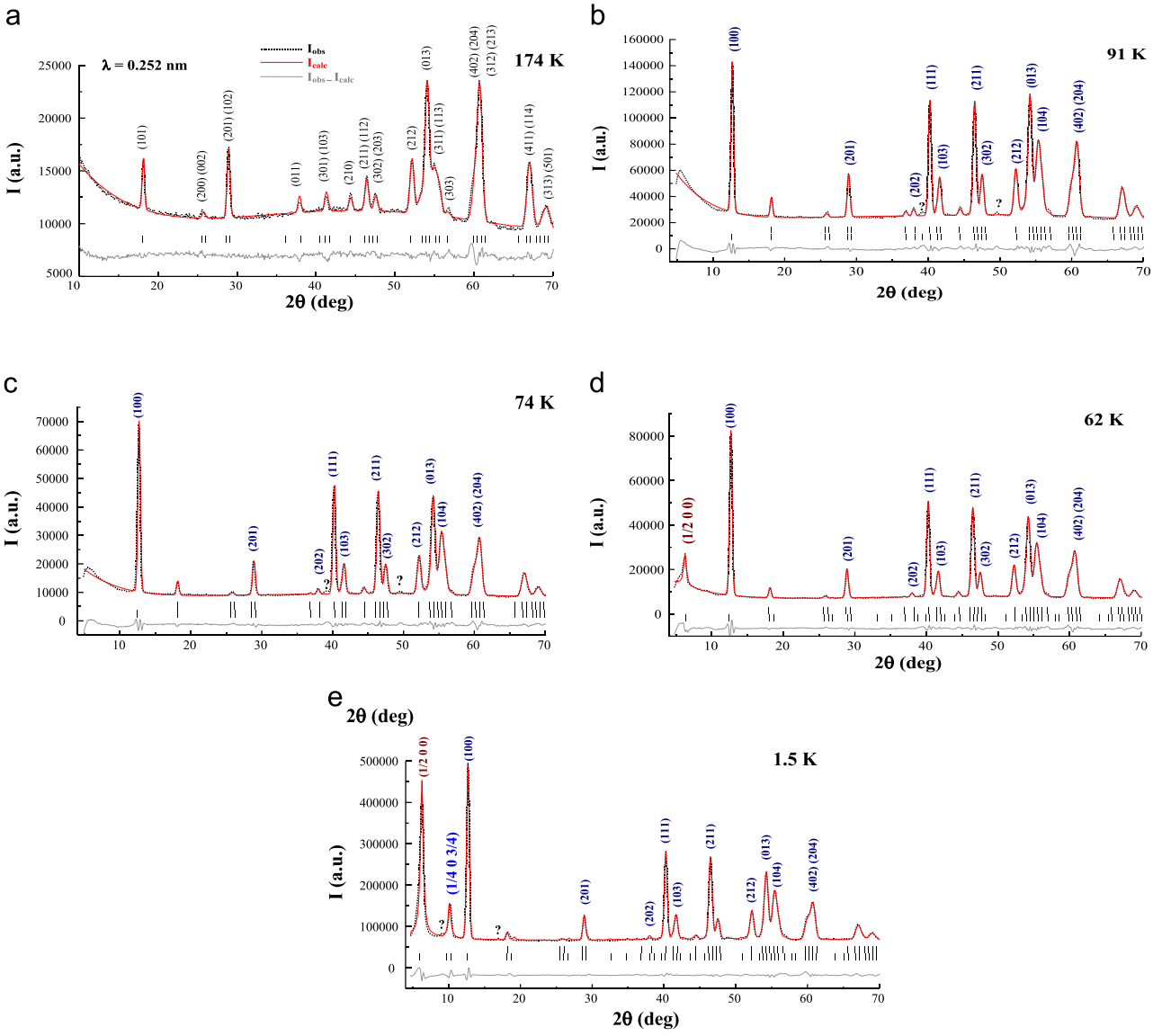

Fig. 3. Neutron diffraction patterns of Tb_3NiSi_2 (a) at 174 K (paramagnetic state), (b) at 91 K (mixed F-AF ordering of ($\mathbf{M}_{ac}^{K0}+\mathbf{M}_b^{K0}$) of the $\mathbf{P2_1'/a}$ magnetic space group), (c) at 74 K (mixed F-AF ordering of $\mathbf{M}_{ac}^{K0}$ of the **Pn′ma** magnetic space group), (d) at 62 K (mixed F-AF ordering with $\mathbf{M}_{ac}^{K0}$ (**Pn′ma**) and $\mathbf{M}_b^{K1}$ magnetic components) and (e) at 1.5 K (mixed F-AF ordering with $\mathbf{M}_{ac}^{K0}$ (**Pn′ma**), $\mathbf{M}_b^{K1}$ and $\mathbf{M}^{K2}$ magnetic components). The wave vectors are $\mathbf{K}_0=[0, 0, 0]$, $\mathbf{K}_1=[1/2, 0, 0]$ and $\mathbf{K}_2=[\pm 1/4, 0 \pm 3/4]$. The upper and lower ticks indicate the structural and magnetic peaks of Tb_3NiSi_2, respectively. The unindexed peaks marked by "**?**" in (b, c and e).

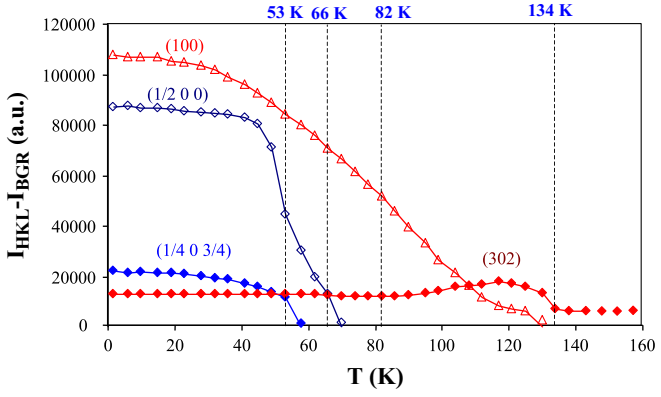

Fig. 4. Thermal evolution of the strongest magnetic reflections with the $\mathbf{K}_0$, $\mathbf{K}_1$ and $\mathbf{K}_2$ wave vectors in the neutron diffraction patterns of Tb_3NiSi_2. Transformation temperatures of the magnetic structure are given at the top.

F-AF ordering with the ($\mathbf{M}_{ac}^{K0}+\mathbf{M}_b^{K0}$) ($\mathbf{P2_1'/a}$) component and magnetic unit cell of $a_{Tb3NiSi2} \times b_{Tb3NiSi2} \times c_{Tb3NiSi2} \rightarrow ac$-plane F-AF ordering with the $\mathbf{M}_{ac}^{K0}$ (**Pn′ma**) component and magnetic unit cell of $a_{Tb3NiSi2} \times b_{Tb3NiSi2} \times c_{Tb3NiSi2} \rightarrow$ sum of the $\mathbf{M}_{ac}^{K0}$(**Pn′ma**) and $\mathbf{M}_b^{K1}$ components with a magnetic unit cell of $2a_{Tb3NiSi2} \times b_{Tb3NiSi2} \times c_{Tb3NiSi2} \rightarrow$ sum of $\mathbf{M}_{ac}^{K0}$(**Pn′ma**), $\mathbf{M}_b^{K1}$ and $\mathbf{M}^{K2}$ components with magnetic unit cell of $8a_{Tb3NiSi2} \times b_{Tb3NiSi2} \times 4c_{Tb3NiSi2}$.

The magnetic ordering below ~130 K can be associated with the first anisotropic distortion of the unit cell ($\Delta a/a_{174\ K} > \Delta b/b_{174\ K} \approx \Delta c/c_{174\ K}$) and the first local maximum in the *V–T* plot. Decrease in the $\mathbf{M}_b^{K0}$ ferromagnetic component below ~117 K coincides with the second anisotropic distortion of the unit cell ($\Delta a/a_{174\ K} > \Delta b/b_{174\ K} > \Delta c/c_{174\ K}$) and the second local maximum in the *V–T* plot (Figs. 2 and 6). The other local maximum in the *V–T* dependence corresponds to the transformation of the magnetic structure at 53 K and increase of the magnetic unit cell to $8a_{Tb3NiSi2} \times b_{Tb3NiSi2} \times 4c_{Tb3NiSi2}$.

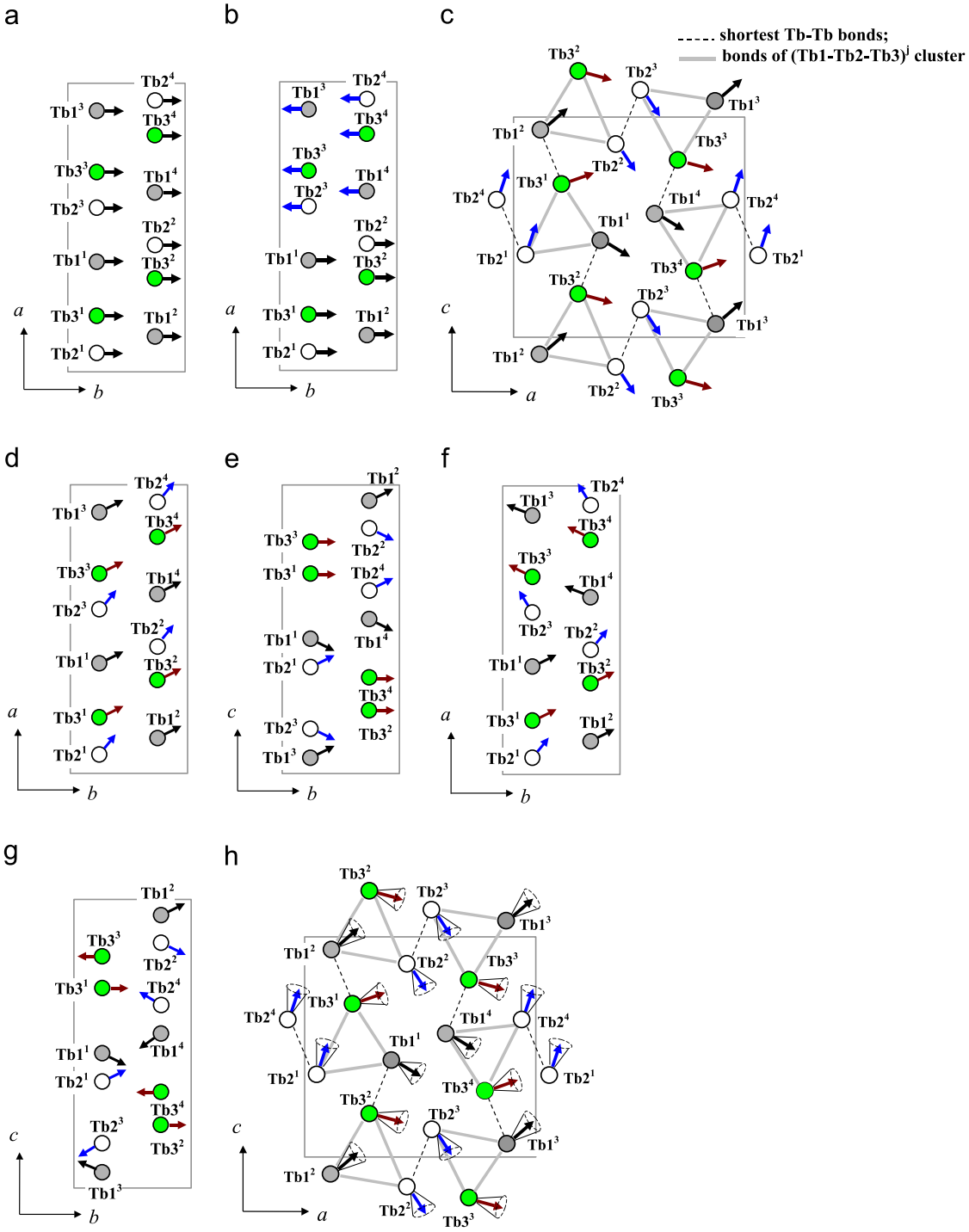

Fig. 5. Magnetic components of the Tb_3NiSi_2 magnetic structure: (a) $\mathbf{M}_b^{K0}$ magnetic component of the **Pnm′a** magnetic space group, (b) $\mathbf{M}_b^{K1}$ magnetic component and (c) $\mathbf{M}_{ac}^{K0}$ magnetic component of the **Pn′ma** magnetic space group. Projections of the magnetic structure of Tb_3NiSi_2 between ~130 K and 82 K (sum of $\mathbf{M}_{ac}^{K0}$ (**Pnm′a**)+$\mathbf{M}_{ac}^{K0}$ (**Pn′ma**) components) are given in (d and e). Between 82 K and 66 K, the magnetic structure is the $\mathbf{M}_{ac}^{K0}$ (**Pn′ma**) magnetic component (c). Between 66 K and 53 K, magnetic structure is the sum of the $\mathbf{M}_{ac}^{K0}$ (**Pn′ma**) and $\mathbf{M}_b^{K1}$ magnetic components (f and g) and below 53 K, the magnetic structure becomes the set of the canted ferromagnetic cones (sum of the $\mathbf{M}_{ac}^{K0}$ (**Pn′ma**), $\mathbf{M}_b^{K1}$ and $\mathbf{M}^{K2}$ magnetic components (h). One unit cell is shown for all types of ordering. The wave vectors are $\mathbf{K}_0$=[0, 0, 0], $\mathbf{K}_1$=[1/2, 0, 0] and $\mathbf{K}_2$=[± 1/4, 0 ± 3/4].

The magnetic structure of Tb_3NiSi_2 is similar to that of Tb_3NiGe_2 [6], when $\mathbf{M}_b^{K0} \gg \mathbf{M}_{ac}^{K0}$ below ~130 K, and to the magnetic structure of {Pr, Nd}$_3CoGe_2$ [5] between 82 K and 66 K (Fig. 5a and c). But contrary to Tb_3NiGe_2 and {Pr, Nd}$_3CoGe_2$, Tb_3NiSi_2 shows four different types of magnetic ordering resulting from the complex RKKY exchange interactions. In addition, the magnetic structure of Tb_3NiGe_2 differs from that of Tb_3NiSi_2, except for a short temperature interval below ~130 K. The temperature of the ferromagnetic ordering in Tb_3NiGe_2 is close to that of Tb_3NiSi_2, but differs from temperature of ferromagnetic transition of La_3NiGe_2-type Tb_3CoGe_2 (T_C=110 K) [2]. Thus, it appears that in such structure, as a rule the transition metal atoms do not carry any magnetic moment and do not influence much the magnitude of the magnetic ordering temperature; whereas the nature of the *p* element plays a determinant role in the observed type of magnetic ordering in the compounds with the La_3NiGe_2-type structure.

Table 4
Crystallographic and magnetic parameters of La_3NiGe_2-type Tb_3NiSi_2 at different temperatures: cell parameters; $\mathbf{M}_{ac}^{K0}$, $\mathbf{M}_{ac}^{K0}$, $\mathbf{M}_b^{K1}$ and $\mathbf{M}^{K2}$ are the Tb magnetic moment with $\mathbf{K}_0=[0, 0, 0]$, $\mathbf{K}_1=[1/2, 0, 0]$ and $\mathbf{K}_2=[\pm 1/4, 0 \pm 3/4]$ wave vector, $|\mathbf{M}|$ is the magnitude of the terbium magnetic moment. $\theta(\mathbf{M}_{ac}^{K0})$ is the angle between the $\mathbf{M}_{ac}^{K0}$ magnetic moment and c axis (the angle $\varphi(\mathbf{M}_{ac}^{K0})$ of the $\mathbf{M}_{ac}^{K0}$ magnetic moment to the a axis is zero). $\mathbf{M}_b^{K0}$ and $\mathbf{M}_b^{K1}$ are along the b axis, $\mathbf{M}_{ac}^{K0}$ belongs to the ac plane and the cone axis of the $\mathbf{M}^{K2}$ flat spiral component coincides with the $(\mathbf{M}_{ac}^{K0}+\mathbf{M}_b^{K0}+\mathbf{M}_b^{K1})$ vector of the corresponding Tb atom. Reliability factors are: R_F for the crystal structure and R_F^m for the magnetic structure. The data given are for one unit cell.

T (K)	Unit cell data (nm)	R_F (%)	Atom	M_{ac}^{K0} (μ_B)	$\theta(M_{ac}^{K0})$ (deg)	M_b^{K0} (μ_B)	M_b^{K1} (μ_B)	M^{K2} (μ_B)	$\lvert M\rvert$ (μ_B)	R_F^m (%)
298[a]	$a=1.1308(1)$ $b=0.41314(3)$ $c=1.1225(1)$	3.1								
174	$a=1.1279(2)$ $b=0.41206(5)$ $c=1.1195(2)$	5.4								
112	$a=1.1288(2)$ $b=0.41168(5)$ $c=1.1184(2)$	4.1	$Tb1^1$, $Tb1^4$ $Tb1^2$, $Tb1^3$ $Tb2^1$, $Tb2^4$ $Tb2^2$, $Tb2^3$ $Tb3^1$, $Tb3^4$ $Tb4^2$, $Tb4^3$	3.34(7) 3.34(7) 3.34(7) 3.34(7) 3.34(7) 3.34(7)	101(2) 79(2) 58(2) 122(2) 90 90	4.18(8) 4.18(8) 4.18(8) 4.18(8) 4.18(8) 4.18(8)			5.35(8)	4.2
74	$a=1.1295(2)$ $b=0.41142(5)$ $c=1.1168(2)$	3.9	$Tb1^1$, $Tb1^4$ $Tb1^2$, $Tb1^3$ $Tb2^1$, $Tb2^4$ $Tb2^2$, $Tb2^3$ $Tb3^1$, $Tb3^4$ $Tb4^2$, $Tb4^3$	7.16(7) 7.16(7) 7.16(7) 7.16(7) 7.16(7) 7.16(7)	111(1) 69(1) 53(1) 127(1) 83(1) 97(1)					2.0
62	$a=1.1297(2)$ $b=0.41135(5)$ $c=1.1165(2)$	3.7	$Tb1^1$ $Tb1^2$ $Tb1^3$ $Tb1^4$ $Tb2^1$ $Tb2^2$ $Tb2^3$ $Tb2^4$ $Tb3^1$ $Tb3^2$ $Tb3^3$ $Tb3^4$	7.99(8) 7.99(8) 7.99(8) 7.99(8) 7.99(8) 7.99(8) 7.99(8) 7.99(8) 7.99(8) 7.99(8) 7.99(8) 7.99(8)	111(1) 69(1) 69(1) 111(1) 50(1) 130(1) 130(1) 50(1) 81(1) 99(1) 99(1) 81(1)		0.99(2) 0.99(2) −0.99(2) −0.99(2) 0.99(2) 0.99(2) −0.99(2) −0.99(2) 0.99(2) 0.99(2) −0.99(2) −0.99(2)		8.05(8)	2.7
1.5	$a=1.1305(2)$ $b=0.41122(3)$ $c=1.1157(1)$	3.5	$Tb1^1$ $Tb1^2$ $Tb1^3$ $Tb1^4$ $Tb2^1$ $Tb2^2$ $Tb2^3$ $Tb2^4$ $Tb3^1$ $Tb3^2$ $Tb3^3$ $Tb3^4$	8.5(1) 8.5(1) 8.5(1) 8.5(1) 8.5(1) 8.5(1) 8.5(1) 8.5(1) 8.5(1) 8.5(1) 8.5(1) 8.5(1)	112(1) 68(1) 68(1) 112(1) 46(1) 134(1) 134(1) 46(1) 79(1) 101(1) 101(1) 79(1)		2.50(5) 2.50(5) −2.50(5) −2.50(5) 2.50(5) 2.50(5) −2.50(5) −2.50(5) 2.50(5) 2.50(5) −2.50(5) −2.50(5)	2.00(5) 2.00(5) 2.00(5) 2.00(5) 2.00(5) 2.00(5) 2.00(5) 2.00(5) 2.00(5) 2.00(5) 2.00(5) 2.00(5)	9.1(1)	3.5

[a] X-ray data.

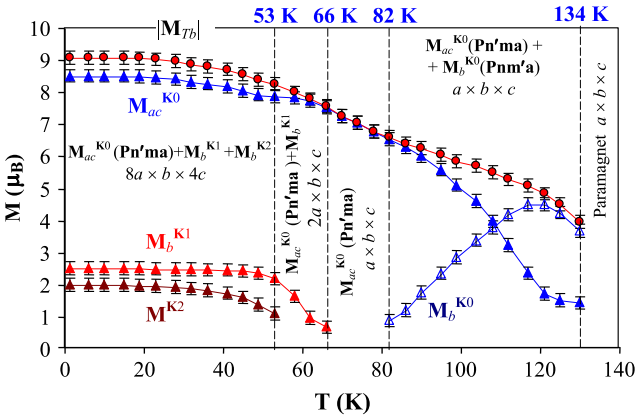

Fig. 6. Thermal evolution of the $\mathbf{M}_b^{K0}$, $\mathbf{M}_{ac}^{K0}$, $\mathbf{M}_b^{K1}$ and $\mathbf{M}^{K2}$ magnetic components of Tb_3NiSi_2 and overal $|\mathbf{M}_{Tb}|$ terbium magnetic moment. The temperatures of the magnetic transformations, type of the magnetic structure and size of the corresponding magnetic unit cell are given in figure.

It is however noticeable that the lower T_C observed for Tb_3CoGe_2 comparison with that of Tb_3NiGe_2, may result from a change of the RKKY exchange interactions as may be expected by the modification of the Tb–Tb interatomic distances as well as the expected change of the electronic density at the Fermi level resulting from the Ni for Co substitution.

4. Conclusions

The mixed antiferro–ferromagnetic nature of La_3NiGe_2-type Tb_3NiSi_2 magnetic structure is clearly demonstrated both from the magnetization and neutron diffraction studies. Analysis of the powder neutron diffraction data reveals that Tb_3NiSi_2 exhibits a complex magnetic phase diagram with several different magnetic orderings of the terbium sublattice upon cooling. The a lattice parameter of Tb_3NiSi_2 increases, whereas the b and c ones and unit cell volume decrease with the decreasing temperature in the magnetically-ordered state. Tb_3NiSi_2 should demonstrate metamagnetic-like transitions in

the applied field, like the other rare earth compounds with mixed F-AF ordering (see f.e. [12]). The Tb_3NiSi_2-based solid solution may be interesting from the point of view of magnetostriction effect.

Acknowledgments

The Institute Laue Langevin is warmly acknowledged for the use of the neutron diffraction beam. This work was supported by the Russian Fund for Basic Research through the Project no. 12-03-00428-a.

References

[1] Pearson's Handbook of Crystallographic Data for Intermetallic Phases, American Society for Metals, Materials Park, OH 44073, 1985, pp. 1–3.
[2] P. Manfrinetti, A.V. Morozkin, O. Isnard, F. Wrubl, Y. Mozharivskyj, V. Svitlyk, Intermetallics 19 (2011) 321–326.
[3] A.V. Morozkin, Jinlei Yao, Y. Mozharivskyj, O. Isnard, Journal of Magnetism and Magnetic Materials 324 (2012) 2977–2982.
[4] F. Izumi, in: R.A. Young (Ed.), The Rietveld Method, Oxford University Press, Oxford, 1993 (chapter 13).
[5] ⟨www.ill.eu⟩, Yellow Book.
[6] J. Rodriguez-Carvajal, Physica B 192 (1993) 55–69.
[7] J. Emsley, The Elements, Second edition, Clarendon Press, Oxford, 1991.
[8] S. Legvold, Rare earth metals and alloys, in: E.P. Wohlfarth (Ed.), Ferromagnetic Materials, North-Holland Publish. Comp., Amsterdam, 1980, pp. 183–295.
[9] P.S. Kireev, Introduction to the Theory Group and it's Application in Solid State Physic, High School, Moscow, 1979. (In Russian).
[10] C.J. Bradley, A.P. Cracknell, The Mathematical Theory of Symmetry in Solids, Clarendon, Oxford, 1972.
[11] O.V. Kovalev, Representations of the Crystallographic Space Groups, second edition, Gordon and Breach Science Publishers, 1993.
[12] A.V. Morozkin, Jinlei Yao, Y. Mozharivskyj, Journal of Solid State Chemistry 192 (2012) 371–376.